Unifying ENDOR, electrochemical, and FTIR spectroscopic results for the Special-Pair radical cation in bacterial photosynthesis

J. R. Reimers[1], A.P. Rendell[2], and Noel S. Hush[1,3]

[1]*School of Chemistry, University of Sydney, NSW 2006, AUSTRALIA*
[2]*Department of Computer Science, Australian National University, ACT 0200 AUSTRALIA*
[3]*Department of Biochemistry, University of Sydney, NSW 2006, AUSTRALIA.*
Email: reimers@chem.usyd.edu.au Fax 61-2-93513329

1. Introduction.

The properties of the radical cation P^+ of the special pair in photosynthetic reaction centres have considerable influence over the process in which optical energy is converted into electrical energy and thence into chemical energy. The reaction centre in purple bacteria is the best understood of all photosynthetic reaction centres, and it is clear that significant differences occur between this and the analogous units in photosystems PS-I and PS-II. It is hence very important that a clear interpretation be obtained of the extensive data available for the bacterial system.

Of particular importance is the degree of charge localization of the cation radical on one of the two halves of the special pair. This has been accessed using three different types of experimental techniques, and we are concerned with the mutual consistency of the results. These techniques are: ENDOR electron-spin resonance spectroscopy [Lin 1994, Artz 1997, Ivancich 1998], electrochemistry [Artz 1997, Ivancich 1998], and FTIR difference spectroscopy [Breton 1992, Nabedryk 1993, Breton 1999]. From the ENDOR work it has been concluded that for the wild-type reaction centre of *Rhodobacter sphaeroides* the charge is localized 70% on P_L, intermediate between what is expected for full localization (100%) and full delocalization (50%). While the electrochemical midpoint potential analysis is consistent with this, the optical spectroscopic results lead to the conclusion [Reimers 1995] that the charge is 94-98% localized on P_L, a strikingly different result.

Our primary aim is to find a mutually consistent interpretation of the entire data set. For all 3 techniques, the degree of localization is obtained using models for the interpretation of the raw data. For ENDOR, this involves assignment of the observed resonance signals to individual atoms, as well as the assumption that the charge density is the same as the spin density. For the electrochemical data, this involves use of a two-state model to interpret the energetics. The spectroscopic data is also interpreted using a similar model first introduced by Hush [Hush 1967], that has been extremely successful in interpreting chemical and biochemical spectra.

Our approach was to examine the assumptions used in the analysis of each experiment.   A complete pictorial description of the 11 major steps in this process has been given elsewhere [Reimers 2000].   This work, as initially envisaged, is approaching completion. Scenarios for the breakdown of the ENDOR analysis were considered, a small but highly significant improvement was made in the analysis of

the electrochemical data, and a dramatically improved analysis of the spectroscopic data involving a complete *a priori* vibronic coupling simulation of the observed spectrum was performed. This spectrum includes both absorption to the first electronic state at a band maximum of ca. 2600 cm^{-1} (3900 nm) as well as the underlying vibrational absorption spectrum. The vibrational spectrum is enhanced with the vibronic coupling between the ground and first excited states giving rise to strong additional *phase phonon* lines which form a key part of the overall spectrum.

Figure 1 The 2600 cm-1 band and its 2200 cm-1 shoulder

2. The hole-transfer and tripdoublet states

Our first task [Reimers 1995] was to provide an assignment for all of the bands observed in the absorption spectrum of P$^+$. The 2600 cm^{-1} band, first observed by Breton *et al.* [Breton 1992], is the hole-transfer absorption band. Using a localized description of the electronic states, this band moves the radical cation hole from one dimer half to the other, ie., from P$_L^+$P$_M$ to P$_L$P$_M^+$; using a delocalized description, it interconverts the symmetric and antisymmetric combinations of the wavefunction of the hole, ie., from a state of symmetry ^{2}B to one of symmetry ^{2}A.

The second lowest-energy electronic absorption is a band found at ca. 8000 cm^{-1} (1250 nm). This was first observed in 1970 but no assignment was available. We assigned it [Reimers 1995a] to a tripdoublet band [Reimers 1994]. Using a localized description, this band can be thought of as the ^{3}Q absorption of a monomeric Bchl (P$_M$) in the presence of a nearby doublet ion (P$_L^+$). It is actually a two-electron transition that is formally forbidden which gains intensity via electronic coupling to the nearby hole-transfer band. It is an extremely unusual electronic transition that can occurs in dimer cation radicals, though similar effects such as the intensification of the triplet absorption of a neutral molecule in the presence of a triplet sensitizer such as O$_2$ are well known. An ENDOR or related study of its properties would show that two thirds of the excess spin density lies on the half which is neutral and only one third lies on the radical cation. If this state mixes with the nearby ground state, standard ENDOR analysis of its charge distribution would give erroneous results. Also, if this state mixes with either the ground or hole-transfer states, then analyses of the FTIR spectrum such as the one we employ would also be in error. It is currently believed that the actual mixing is quite low, but further work is required.

3. The 2200 cm^{-1} shoulder of the hole-transfer band

The hole-transfer band, centred near 2600 cm^{-1}, is skewed to low frequency and has a shoulder at ca 2200 cm^{-1}, see Figure 1. Electronic absorption bands are either symmetric or skewed to high frequency, and no explanation of the 2200 cm^{-1} shoulder as a part of the main band is apparent. We examined [Reimers 1998] the experimental data available in 1998 [Breton 1992, Nabedryk 1993] (Fig. 1) and concluded that its behaviour as a function of environment was suggestive that the shoulder is part of an independent electronic. Polarization studies [Wynne 1996] support this conclusion, but it needs to be reinvestigated in the light of recent experimental data shown at this conference by Boxer, Breton, Hastings, and others.
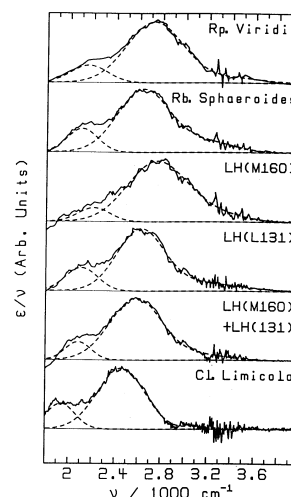
4. Vibronic coupling between electronic states

Vibronic coupling results in non-adiabatic vibrational wavefunctions, ie., ones that cannot be described as belong-ing to a single electronic state. It may be approached in one of three equivalent ways [Reimers 1996], starting with electronic states that are either localized diabatic, delocalized diabatic, or adiabatic in nature, as indicated in Fig. 2 for the simple case in which the dimer is symmetric (here, C_2 symmetry). For the diabatic cases, one term in the electronic energy is ignored, this being the inter-dimer coupling J in the localized case and the antisymmetric-mode reorganization energy λ in the other. Diagonalizing parametrically the electronic-only Hamiltonian produces, in both cases, the adiabatic potential-energy surfaces which have two characteristic shapes depending on the balance of the coupling and reorganization energies, see Fig. 2.

The full vibronic coupling problem is difficult to solve using adiabatic states, and we have tried both diabatic representations. In the localized approach, the $P_L^+P_M$ and $P_LP_M^+$ states have different equilibrium geometries which we represent in terms of dimensionless displacements λ_i in terms of the normal modes of frequency ν_i. Each vibrational level in each electronic state becomes coupled to all levels in the alternate electronic state by Franck-Condon vibrational overlap factors scaled by the electronic coupling J. Unfortunately, for problems such as the special-pair radical cation in which a large number of vibrational modes are implicated, this representation yields a Hamiltonian matrix containing an extremely large number of extremely small terms whose net effect is important, rendering its solution technically infeasible. In the delocalized approach, the vibrational levels of the ^2B and ^2A diabatic states are coupled through vibronic couplings α_i. Because of the selection rules in operation, almost all of the Hamiltonian matrix elements are zero in this representation, making it suitable for the current application. The vibronic coupling constants and reorganization energy components are easily related to the displacements appearing in the localized description through $\lambda_T = \sum_i \lambda_i$, $\lambda_i = 2h\nu_i\delta_i^2$, $\alpha_i = h\nu_i\delta_i$.

Figure 2 Various representations of vibronic coupling

In reaction centres, the dimer halves are asymmetric and this is modelled using an energy offset E_0 related to the difference in midpoint potentials for the dimer halves in the absence of inter-dimer coupling. Its effect is readily envisaged in the localized diabatic representation shown in Fig. 3; in the delocalized diabatic representation, the asymmetry results [Reimers 1996] in displacements of the ^2B and ^2A wells in antisymmetric normal coordinates, see Fig. 3.
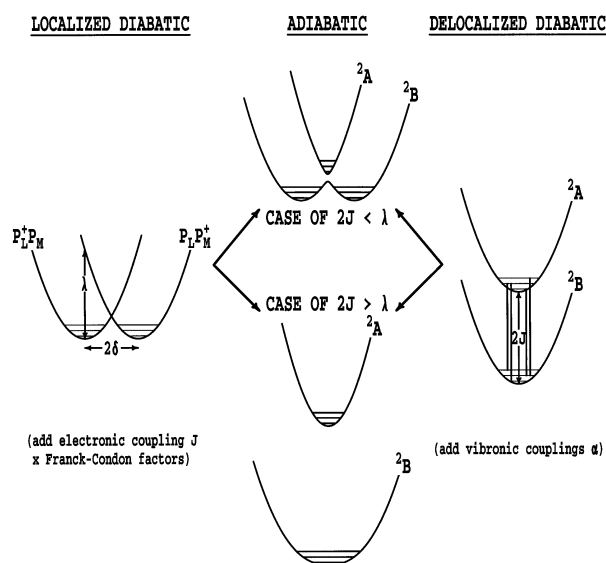
5. Results of early model calculations

The FTIR cation-minus-neutral difference spectrum observed by Breton *et al.* [Breton 1999], shown later in Fig. 6, contains a large number of both positive-going and negative-going peaks. Pairs of these arise from intense absorptions whose frequency is changed on oxidation, but other peaks are new and are phase phonon lines which highlight the individual

Figure 3 Including energy asymmetry E_0 in the vibronic coupling model

vibrational modes participating in the vibronic coupling. Originally, only 3 clear phase-phonon lines were identified. The spectrum shown [Breton 1999] extends down to 400 cm^{-1} and has a clearly defined baseline, but the spectra initially obtained [Breton 1992, Nabedryk 1993] commenced at 1200 cm^{-1} and the location of the baseline was uncertain. We indicated the importance of the location of the baseline and the low-frequency region to the interpretation of the spectrum [Reimers 1995], prompting an extensive redesign of the experimental apparatus [Breton 1999]. Our conclusions were based on model vibronic coupling calculations which included 1-3 high-frequency modes and 1 low frequency mode, the simplest approaches consistent with the available experimental data. The conclusions drawn from these calculations differed markedly depending on assumptions concerning the location of the baseline, but the most probable conclusion was that the phase-phonon intensity, as well as the electronic band intensity and width, could all be modelled using optimized parameters such as $J = 0.053$-0.081 eV, $\lambda = 0.092$ eV, and $E_0 = 0.25$ eV, leading to the conclusion that the electronic charge is highly localized.

Our exploratory calculations included only the ground and hole-transfer states and so remained within the spirit of the original 2-state model of Breton [Breton 1992]; they extended the original calculations in that the band width could be simultaneously modelled. We investigated general properties of tripdoublet states [Reimers 1994] and found that the tripdoublet intensity derives primarily from that of the hole-transfer band. As these states are observed to have similar intensity, the implication is that the hole-transfer band intensity which should be used fitting in the vibronic coupling results should be ca. twice that actually observed. As a result, we repeated the calculations [Reimers 1996] examining the entire parameter space, depicting regions which were consistent with either all of the experimental data or all data except the intensity information, and the results are shown in Fig. 4. Within the larger region, a spot consistent with the ENDOR data is found with 70% charge localization, $J = \lambda = 0.16$ eV, and $E_0 = 0.075$ eV.
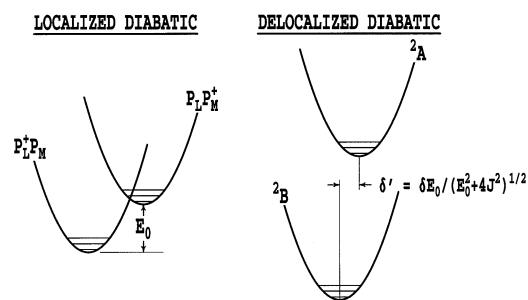

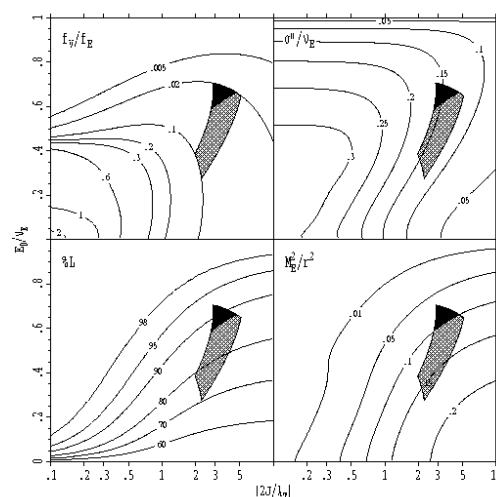**Figure 4** Solution of a 1-mode vibronic coupling model showing the % charge on P_L, the electronic transition moment M_E, the bandwidth σ", and phase-phonon to electronic intensity ratio f_v / f_E. Dark- fit using all exp. data; gray- fit ignoring M_E

6. Obtaining values for the vibronic coupling parameters J, E_0, and all ν_i and λ_i

We calculated values for J and the vibrational frequencies and reorganization energies using a gas phase dimer of C_2 symmetry of a model BChl compound consisting of BChl with all side chains removed and an imidazole ligand added. Its geometry in the ^1A neutral ground state and ^2B and ^2A cation radical ground and hole transfer states were optimized using B3LYP/3-21G and vibration frequencies and transition moments obtained. Electronic coupling J were then obtained at higher levels of theory using these geometries [Reimers 2000] and were in the range 0.07 - 0.11 eV. However, it was clear that the B3LYP/3-21G geometries overestimated the ring-I to ring-I separations and hence J could be significantly underestimated. This result was not of sufficient quality to be useful in our full spectral simulations, but we employed the calculated vibration frequencies and coupling constants deduced from the transition moments; the vibronically induced transition moments were all of very similar polarization, suggesting that vibronic coupling to tripdoublet and other states is not important. In Figure 5 is shown the calculated spectrum of vibrationally resolved reorganization energies, and it is clear that a very large number of vibronically active modes are active. The highest frequency coupled mode has pyrrole breathing character; it is of g symmetry in porphyrin and hence forbidden, is very weak in Bchl and $BChl^+$, and very intense in P^+ due to the vibrionic coupling. The low frequency modes are of interest as they have periods commensurate with the rate of electron transfer from P forming P^+. The calculated total reorganization energy is $\lambda_T = 0.20$ eV.
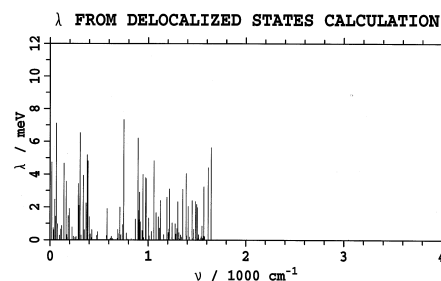

Figure 5 calculated reorganization energy spectrum

Values of J and E_0 have been deduced from experimental midpoint and ENDOR charge density data by Allen *et al.* [Artz 1997, Ivancich 1998]. However, the value of $J = 0.24 \pm 0.04$ eV is larger than the absolute maximum, 0.17 eV, permitted from the intervalence band maximum, with values in excess of 0.15 eV appearing to be highly unlikely. While differential electronic coupling between the ground and hole-transfer states with the tripdoublet states could result in depression of the hole-transfer energy, the effect disappears in first order and hence is not expected to be significant. We revised their analysis [Reimers 2000a] correcting a small mathematical error and obtained more realistic values of $J = 0.18 \pm 0.03$ eV and $E_0 = 0.14 \pm 0.03$ eV. The subsequent spectral simulations are thus performed using $J = 0.15$ eV, $E_0 = 0.14$ eV, and $\lambda_T = 0.20$ eV, near to the region revealed by the prior crude model calculations as the one in which ca. 70% charge localization is expected.
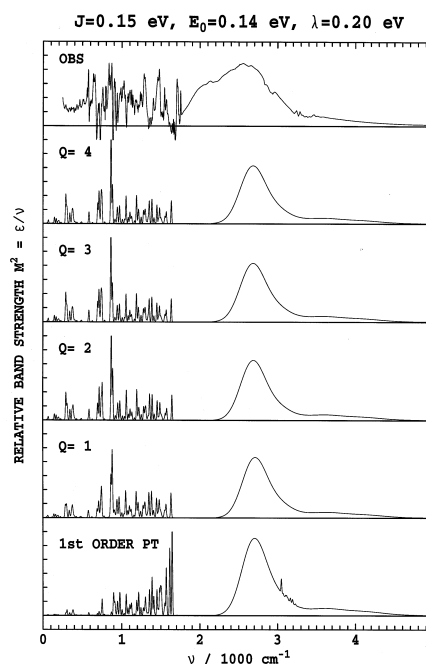
7. *A priori* spectral simulation

The calculation of the vibronic spectrum is of a complexity unprecedented in vibronic coupling calculations. We include 91 active modes and all

Figure 6 Calculated and observed spectra; Q is the truncation level

vibrational levels containing up to $Q = 5$ vibrational quanta. The dimension of the resulting Hamiltonian matrix is then of order 10^9, and we reduce this using (i) an efficient truncation scheme, (ii) by treating all truncated matrix elements and the highest excited quanta using perturbation theory, (iii) treating the effect of E_0 using perturbation theory, and (iv) using time-dependent quantum mechanics [Reimers 1983] to obtain the spectra shown in Fig. 6 at 10 cm^{-1} vibrational and 300 cm^{-1} electronic resolution. The calculated and observed spectra show good agreement concerning the number and distribution of phase-phonon lines, the location and width of the main electronic absorption band at 2600 cm^{-1}, and the length and height of the high-frequency tail. Note that the large differential signals in the observed spectra due to excited-state frequency changes are not yet included in the simulations.

8. Conclusions

Our *a priori* simulations of the phase-phonon structure and hole-transfer band using a consistent parameter set indicates that the ENDOR, electrochemical, and spectroscopic data can be unified to give a common description of the charge delocalization in P^+. The failure of simple theory [Hush 1967] to correctly interpret the spectrum is attributed to intensity stealing by the tripdoublet states from the hole-transfer state, and other issues remain concerning the importance of the hole-transfer states to the process. The identity of the 2200 cm^{-1} shoulder remains unresolved; its nature, as well as the deduce vibrionic coupling properties, are expected to have significant ramifications for the related spectra of PS-I which are just being reported.

9. Acknowledgments

10. References

[Artz 1997]   K. Artz, J.C. Williams, J.P. Allen, F. Lendzian, J. Rautter, and W. Lubitz, *Proc. Natl. Acad. Sci. USA* **94**, 13582 (1997).
[Breton 1992] J. Breton, E. Nabedryk, and W.W. Parson, *Biochem.* **31**, 7503 (1992).
[Breton 1999] J. Breton, E. Nabedryk, and A. Clérici, *Vibrational Spectrosc.* **19**, 71 (1999).
[Hush 1967]   N.S. Hush, *Prog. Inorg. Chem.* **8**, 391 (1967).
[Hutter 1998] M.C. Hutter, J.R. Reimers, and N.S. Hush, *J. Phys. Chem. B* **102**, 8080 (1998).
[Hutter 1999] M.C. Hutter, J.M. Hughes, J.R. Reimers, and N.S. Hush, *J. Phys. Chem. B* **103**, 4906 (1999).
[Hutter 2001] M.C. Hutter, J.M. Hughes, J.R. Reimers, and N.S. Hush, *J. Am. Chem. Soc.* (2001) in press # JA0035710.
[Ivancich 1998] A. Ivancich, K. Artz, J.C. Williams, J.P. Allen, and T.A. Mattioli, *Biochem.* **37**, 11812 (1998).
[Lin 1994] X. Lin, H.A. Murchisson, V. Nagarajan, W.W. Parson, J.P. Allen, and J.C. Williams, *Proc. Natl. Acad. Sci.* **91**, 10265 (1994).
[Nabedryk 1993] E. Nabedryk, J.P. Allen, A.K.W. Taguchi, J.C. Williams, N.W. Woodbury, and J. Breton, *Biochem.* **32**, 13879 (1993).
[Reimers 1983] J.R. Reimers, K.R. Wilson, and E.J. Heller, *J. Chem. Phys.* **79**, 4749 (1983).
[Reimers 1994] J.R. Reimers and N.S. Hush, *Inorg. Chim. Acta* **226**, 33 (1994).

[Reimers 1995] J.R. Reimers and N.S. Hush, *Chem. Phys.* **197**, 323 (1995).

[Reimers 1995a] J.R. Reimers and N.S. Hush, *J. Am. Chem. Soc.* **117**, 1302 (1995).

[Reimers 1996] J.R. Reimers and N.S. Hush, *Chem. Phys.* **208**, 177 (1996).

[Reimers 1998] J.R. Reimers, M.C. Hutter, and N.S. Hush, *Photosynth. Res.* **55**, 163 (1998).

[Reimers 2000] J.R. Reimers, M.C. Hutter, J.M. Hughes, and N.S. Hush, *Int. J. Quant. Chem.* **80**, 1224 (2000).

[Reimers 2000a] J.R. Reimers, J.M. Hughes, and N.S. Hush, *Biochem.* 16185 (2000).

[Wynne 1996] K. Wynne, G. Haran, G.D. Reid, C.C. Moser, P.L. Dutton, and R.M. Hochstrasser, *J. Phys. Chem.* **100**, 5140 (1996).